NIST-GCR-94-642

PREDICTION OF FIRE DYNAMICS

R. L. Alpert and J. de Ris

United States Department of Commerce
Technology Administration
National Institute of Standards and Technology

NIST-GCR-94-642

PREDICTION OF FIRE DYNAMICS

R. L. Alpert and J. de Ris
Factory Mutual Research Corporation
Norwood, MA 02062

Issued June 1994
September 1992

Sponsored by:
U.S. Department of Commerce
Ronald H. Brown, *Secretary*
Technology Administration
Mary L. Good, *Under Secretary for Technology*
National Institute of Standards and Technology
Arati Prabhakar, *Director*

Notice

This report was prepared for the Building and Fire Research Laboratory of the National Institute of Standards and Technology under grant number 60NANB1D177. The statements and conclusions contained in this report are those of the authors and do not necessarily reflect the views of the National Institute of Standards and Technology or the Building and Fire Research Laboratory.

PREDICTION OF FIRE DYNAMICS

FINAL AND FOURTH QUARTERLY REPORT

June 28, 1992 - August 28, 1992

NIST Grant No: 60NANB1D1177

September 1992

R.L. Alpert and J. de Ris
Principal Investigators

Factory Mutual Research Corporation
Norwood, MA 02062

INTRODUCTION

This report summarizes accomplishments of a Factory Mutual Research Corporation (FMRC) project on the Prediction of Fire Dynamics for the NIST grant period August 1991 through August 1992. Work performed under a subcontract by Professor H.W. Emmons on Ceiling-Jet Dynamics and on Development of Strategies for Performance Fire Codes is first described under Task 1. The accomplishment of three tasks performed at FMRC are then presented in summaries of Tasks 2 - 4. All of this work is aimed at the development of subroutines or algorithms that can be used in NIST/BFRL comprehensive computer models.

During the past year, there has been further progress in the development of predictive models for flame radiant heat flux and in the development of a practical laboratory test method for measuring the smoke point of solid noncharring or charring materials. This progress should allow continuing improvements in the accuracy and applicability of fire propagation theories.

Task 1. Prediction of Fire in Buildings (H.W. Emmons, Gordon McKay Professor of Mechanical Engineering Emeritus, Abbott and James Lawrence Professor Engineering Emeritus)

The objective of this task is to advance the knowledge of the science of fire physics, chemistry, psychology, and physiology, so as to make rational quantitative design for fire safety possible.

The two major items worked upon this year were:

1. The simplified theory of ceiling jets.
2. The advancement and use of fire models in fire safety engineering.

1. The Ceiling Jet

Present knowledge of the flow of hot fire gases along a ceiling consists of two parts. Practical engineering generally uses empirical data from some source judged to be equivalent or a field model, used in a few cases where nothing else was possible. The three dimensional field model would be expected to agree excellently with experiment but I know of no detailed check. It is essential for research but too slow and too costly for most practical work.

The wide spread use of field models depends upon future computer cost and availability. They will certainly not be used if there are sufficiently accurate and simpler methods available. We should note that the flow through a nozzle is never computed by a field model. A simple application of Bernoulli's equation plus an empirical coefficient correcting for boundary layers, turbulence, and detailed nozzle design serves all practical purposes. This Task #1 was undertaken to provide a simple method for the ceiling jet.

The conservation of mass, momentum, and energy with assumed top hat velocity and temperature profiles provide what would be expected to be an adequate theory. The success of this expectation ws presented at the third IAFSS meeting at Edinburgh (1) (and Home Fire Project Report #82). For friction and entrainment the theory is adequate (although it cannot always meet a general inlet nor outlet condition) just as is true for hydraulic channel flow. For heat transfer, the solution cannot meet required boundary conditions on either end and does not agree with available experimental results. The inlet conditions are perhaps not too important, but during the transient phase and for an open ended corridor or ceiling the Richardson number must be 1. This has been a most difficult problem which only recently has shown some hope of solution.

If we look at the simplified x momentum equation, it is not obvious that density increase by heat transfer should cause so much trouble. The published reports (1) contain a somewhat complex solution. A far simpler one has recently been found as follows:

$$\dot{m}u_x = -g(\rho_a - \rho)\delta\delta_x + \frac{g\delta^2}{2} R_x \quad \text{(Ref. 1 equation 2)} \qquad 1$$

The right side can be simplified to

$$\dot{m}u_x = \frac{-g}{2} (\delta^2 (\rho_a - \rho))_x \qquad 2$$

which now integrates immediately to

$$\dot{m}u = \frac{-g}{2} (\rho_a - \rho)\delta^2 + c \qquad 3$$

Evaluating the constant of integration at the position where the flow is critical (subscript c) i.e., where Ri = 1

$$c = \frac{3u}{2} \qquad 4$$

and equation 3 reduces to the simple relation

$$Ri = \frac{3u}{u_c} - 2 \qquad 5$$

This relation appears hopeful for the existence of a tranquil flow upstream of Ri = 1, because a decrease of velocity from the critical value $u_c/u > 1$ implies an increase of Ri about 1 which is desired. However if u and u_c are eliminated from equation 5 in terms of Ri, we get

$$\frac{3^3 Ri}{(2 + Ri)^3} = \left(\frac{T - T_a}{T_c - T_a}\right)\frac{T}{T_c} \qquad 6$$

Since the left side has a maximum at Ri = 1 (see Figure 3 of #82 of Ref 1), a real solution of Ri exists only for $T < T_c$ i.e. locations downstream of Ri = 1.

To see what is happening, equation 3 is expressed in terms of $\eta = \delta/\delta_c$, $R_a = \rho_a/\rho_c$, $R = \rho/\rho_c$

$$\frac{(R_a - R)R}{(R_a - 1)}\eta^3 - 3R\eta + 2 = 0 \qquad 7$$

This has been plotted in Figure 1 for three cases

R = 1.5, R = .5 $\rho < \rho_c$ upstream of Ri = 1
R = 1.5, R = 1 $\rho = \rho_c$ at critical
R = 1.5, R = 1.3 $\rho > \rho_c$ downstream of Ri = 1

We see that upstream of Ri = 1 there is only one real root and this at negative depth. Downstream of Ri = 1 there are three real roots one with tranquil flow, one with shooting flow and an unreal negative depth. Within the top hat theory there are no solutions which can describe a ceiling jet with assorted downstream conditions.

To see how nature, in the form of Chobotov's careful experiments (2), manages to avoid the large increase of Ri predicted by the simple theory, the terms of the x momentum and energy equations (8,9) were evaluated by plotting u, $\delta^2(\rho_a - \rho)$, and $(T - T_a)$

$$\dot{m}u_x = -g(\delta^2(\rho_a - \rho))_x - f\rho u^2 \qquad 8$$

$$\dot{m}c_p(\ell n(T - T_a))_x = -h \qquad 9$$

and graphically measuring their slopes and thus evaluating the effective f and graphically measuring their slopes and thus evaluating the effective f = $\tau/1/2\rho u^2$ and St = $\dot{q}''/\rho u c_p \Delta T$. The results are given (ℓn-ℓn) as functions of Reynolds number on Figure 2. The values are nearly constant (f = .0652, St = .0408) for the first two meters of the experimental 5 meter channel and then fell to f = .046, St = .030. The values of the friction factor are much larger than seems reasonable for these boundary layer flows. These high values probably include some of the effects of the top hat assumption and the fact that the experiment did satisfy all the boundary conditions which the simple theory cannot do.

Where things stand now is that practical work must either continue to compute the ceiling jet by a field theory or use the available empirical results from some source judged to be equivalent.

AN ENHANCED TOP HAT THEORY

One might think that the next more complex theory to the simple top hat assumption might be one with a more realistic velocity and temperature profiles. These changes cannot improve the ability to meet inlet and outlet or leading edge requirements. This was inadvertently shown by Chobotov in his thesis not to be true. He developed such a theory which failed to agree with his experiments. To satisfy the required boundary conditions it is essential for the momentum equation normal to the ceiling y to force required depth changes to meet inlet and outlet conditions.

Although a few of the resultant formulas have been given in progress reports, no hint was given as to how they were obtained. This will be briefly done in the following.

For the present we assume steady flow and neglect the effect of friction on the y flow component. The basic momentum equations are:

$$(\rho u^2)_x + (\rho uv)_y = -p_x - F \qquad 10$$

$$(\rho v^2)_y + (\rho vu)_x = -p_y + \rho g \qquad 11$$

The top hat assumptions made are:

1. u, T independent of y to depth δ
2. $v = u\delta_x\, y/\delta$ 12

which assumes v to be a component of u produced by the change of depth of the layer surface which then decreases linearly to zero at the ceiling. Substituting 12 into 11 gives for the vertical pressure gradient within the ceiling jet,

$$p_y = \rho g - \left(\frac{\rho u^2 (\delta_x)^2 y^2}{\delta^2}\right)_x - \left(\frac{\rho u^2 \delta_x y}{\delta}\right)_x \qquad 13$$

of which the first term on the right is the usual hydrostatic effect while the next two terms are y momentum adjustments. The pressure throughout the ceiling jet is found by integration of equation 13 from y to δ (since the pressure is known at δ but not at the ceiling.)

$$-p(x,y) = -p(\delta) + \rho g(\delta - y) - (\rho u^2 \delta\delta_x)_x \frac{(\delta^2 - y^2)}{2\delta^2} \qquad 14$$

note that the last two terms of equation 13 have been combined after the y integration. The x momentum equation now becomes

$$(\rho u^2)_x + \left(\frac{\rho u^2 \delta_x y}{\delta}\right)_x = -(p(\delta))_x + (\rho g(\delta - y))_x - \left((\rho u^2 \delta \delta_x)_x \frac{(\delta^2 - y^2)}{2\delta^2}\right)_x - F \quad 15$$

and now the x momentum equation for the ceiling jet is obtained by integrating equation 15 in y from 0 to $\delta(x)$. After some effort to combine terms the final x momentum equation for the ceiling jet is

$$(\rho u^2 \delta)_x = \frac{-g((\rho_a - \rho)\delta^2)_x}{2} - \frac{(\rho u^2 \delta^2 \delta_x)}{3}_{xx} - \frac{f\rho u^2}{2} \quad 16$$

This form of the momentum equation is simpler than previously published and has not yet been extensively explored.

For the case of no friction, heat transfer, nor entrainment, equation 16 can be integrated. The differential equation becomes:

$$\eta_{zzz} + 3\left(\frac{1}{\eta}\right)_z + \frac{3}{2}(\eta^2)_z = 0 \quad 17$$

where $\eta = \delta/\delta_c$, $z = x/\delta_c$, and subscript c refers to the critical condition.

Equation 17 has the solution

$$\frac{L}{\delta_c} - z = \int_1^{\eta} \frac{d\eta}{\sqrt{2}\left(C_2 + C_1\eta - 3\ell n\ \eta - \frac{\eta^3}{2}\right)^{1/2}} \quad 18$$

where $c_1 = (\eta_{zz})_c + 4.5$ 19

$$c_2 = (\eta_z)_c^2/2 + 1/2 - c_1 \quad 20$$

and the integration starts at $z = L/\delta_c$; the open end of a corridor or the leading edge of a transient ceiling jet.

If the integration is started at the end and computes the ceiling jet depth back to the source which is far away, the denominator must approach zero. Since the denominator contains a square root, a zero denominator is not sufficient since the integration of a reciprocal square root is finite for all

finite η. Thus to have a ceiling jet of small finite depth back to a distant source requires that the denominator and its derivative must both be zero. Thus for a finite source of depth $\eta 1$

$$c_1 = 3/\eta 1 + 1.5\ \eta 1^2 \qquad 21$$

$$c_2 = -c_1\eta 1 - 3\ell n\ \eta 1 + .5\eta 1^3 \qquad 22$$

The values of c_1, c_2 and the ceiling jet slope and curvature at the critical point are plotted in Figure 3. The most important result is the value limits set for the critical ceiling jet slope $(\eta_z)_c$. There is a real slope for shooting flows, $\eta 1 < 1$, but only imaginary values for tranquil flow. This is the effect of the square root. This limitation of the flow to shooting flows is in agreement with a remark by Zukoski who said that the Richardson number behind the front of an advancing ceiling jet was usually slightly less than one.

If we now look at the source of a ceiling jet flow we are given in addition to the mass flow rate and density, the depth and the slope of the surface $(\eta_z)_L$. The x momentum equation can be solved exactly as before resulting in the solution:

$$z = \int_{\eta_i}^{\eta} \frac{d\eta}{\sqrt{2}\ (c_2 + c_1\eta - 3\ell n\ \eta - \frac{\eta^3}{3})^{1/2}} \qquad 23$$

Where c_1 and c_2 are again set by the long range ceiling jet depth, $\eta 1$, as in equations 21 and 22. However they are not related to the inlet conditions.

$$c_1 = (\eta_{zz})_i + 3/\eta_i + 1.5\ (\eta_i)^2 \qquad 24$$

$$c_2 = (\eta_z)_i^2/2 + 3\ell n\ \eta_i + .5\eta_i^{1/3} - c\eta_i \qquad 25$$

Again to have the solution contain a finite depth at long range requires that the values of c_1 and c_2 be the same as before. Thus we can see the complete solution process as follows.

The boundary conditions to be satisfied are; critical flow at $z = L/\delta_c$, and $\eta = \eta_i$, $\eta_z = (\eta_z)_i$ at $z = 0$. By inserting equation 21 and 22 into 25 we get

$$(\eta_z)_i^2/2 = 3\ln \eta 1/\eta_i + \frac{\eta 1^2 - \eta_i^2}{2} + \left(\frac{3}{\eta 1} + 3\eta 1^2\right)(\eta_i - \eta 1) \qquad 26$$

from which n1 is computed. c_1 and c_2 are then found from 21 and 22. These constants are then used to compute upstream from $z=L/\delta_c$ by equation 18 and downstream from z = 0 by equation 23. The two solutions are then connected together somewhere in between.

2. Past Activities and Publications Related to the Advancement and Use of Fire Models in Fire Safety Engineering (See Item 7 for an explanation of the use of Table 1 in fire models)

    1. The conference on Fire Safety Design in the 21st Century May 8-10, 1991 at Worcester Polytechnic Institute. Presented the paper "Strategies for Performance Codes in the U.S."
    2. Third Symposium of the IAFSS at Edinburgh July 8-12, 1991 Presented the paper "The Ceiling Jet in Fires".
    3. Participated in the NFPA Model Users Group meeting October 2, 1991 at Worcester Polytechnic Institute.
    4. Presented a seminar on "Fire Science and the New Fire Safety Engineering" October 16, 1991 at Chemical Engineering Seminar Series at MIT.
    5. Participated in the Annual Fire Research Conference October 28-30, 1991 at NIST.
    6. Participated in the CIB meeting October 30 - November 1, 1991 at NIST. Presented the paper "Validating Models and Algorithms".
    7. Presented a tutorial on "Fire Model Applications - the MGM Fire" January 15, 1992 at NFPA Model Users Group meeting at NFPA. Since this was a tutorial, it was important to discuss how to find the model input data and the manner of defining burning objects as clusters of numerous items. A copy of the available input data constants distributed at the meeting is attached as Table 1.
    8. Presented a seminar "The New Fire Safety Engineering" March 26, 1992 at the Mechanical Engineering Seminar Series and the Center for Applied Energy Research at the University of Kentucky.

9. Presented a lecture on "Genesis and Future of Fire Modeling" April 4, 1992 as the first lecturer on the new Howard W. Emmons Distinguished Lecture at Worcester Polytechnic Institute.
10. Presented a seminar "Fire Science and the New Fire Protection Engineering" April 29, 1992 at the Thermal Sciences Seminar Series Mechanical Engineering Department MIT.

REFERENCES

1. H. Emmons, "The Ceiling Jet in Fires," Third International Symposium on Fire Safety Science - also the more detailed version Home Fire Project Technology Report #82, 1991.

2. Chobotov, M.V., Gravity Currents with Heat Transfer Effects, Ph.D. Thesis California Institute. of Technology, 1987.

TABLE I

FIRE DATA

November 22, 1991

Fuel		polyoxymethylene (pom) -CH2O-	polypropylene (pp) -CH2-	polystyrene (ps) -CH-CH2- solid foam		polymethyl methacrylate (pmma) -CH2-C(CH3)-COOCH3	polyethylene (pe) -CH2-	polyurethane (ρu) -N-C-O- H O foam
ρ	density kg.n3	1400	904	1051	16	100	1170	47
k	thermal conductivity w/m°K	.23	.117	.154	.038	.05	.185	.054
c_p	specific heat j/kg°K	1500	2000	1350		2300	2000	1900
H_c*10^{-7}	combustion heat j/kg	1.55	4.65	3.9		4.7	2.52	2.8
H_v*10^{-6}	pyrolysis heat j/kg	2.43	2.03	1.8		1.8	1.63	2.5
T_{ig}	Ignition temperature°K	700	760	750		789	700	580
T_f	Flame temperature°K	1300	1350	1200		1300	1380	1280
γ_s	air fuel ratio (stoi)	4.60	14.8	13.3		14.8	8.28	9.85
γ	air fuel ratio	8	19	16		32.4	14	14.4
ε	emissivity	1	1	1		.9	.92	.98
κ	absorption coef. m^{-1}	.6	2	4		2	1.4	1.4
χ	fraction heat release	.9	.9	.5		.85	.94	.65
χ_R	Fraction heat radiated	.27	.3	.28	4	.3	.3	.3
Δ	burn rate	.0085	.0112	.0187		--	.0133	.0109
$f(CO_2)$	fraction pyro CO_2	1.4	2.8	2.2	2	2.27	2.2	1.7
f(CO)	fraction pyro CO	.002	.025	.07	.02	0.26	.011	.011
f(HC)	FRACTION PYRO (HC)	.002	.002	.006		.1	.002	.005
F(smoke)	fraction pyro	.002	.1	.33	.2	.3	.025	.18
$F(H_2O)$	fraction pyro H_2O	.6	1.29	.686		1.16	.719	.8

FIRE DATA November 22, 1991

Fuel		acetone CH3-C-CH3 " O	heptane C7H16	gasoline (C8H18)	kerosene (C12H26)
ρ	density kg.n3	813	686	720	--
k	thermal conductivity w/m°K	.19	.140	.127	.105
c_p	specific heat j/kg°K	2114	1660	2200	2150
H_c*10^{-7}	combustion heat j/kg	3.08	4.55	4.4	4.30
H_v*10^{-6}	pyrolysis heat j/kg	--	.48	.30	1.8
T_{ig}	Ignition temperature°K	834	488	572	483
T_f	Flame temperature°K	1400	1400	1300	1300
γ_s	air fuel ratio (stoi)	9.45	15.18	14.97	14.99
γ	air fuel ratio	16.6	19	20	28
ϵ	emissivity	.4	1	.42	.42
κ	absorption coef. m^{-1}	1	.85	.87	1.05
χ	fraction heat release	.91	.85	.3	.83
χ_R	Fraction heat radiated	.23	.35	.35	.35
Δ	burn rate	--	--	--	--
$f(CO_2)$	fraction pyro CO_2	1.734	2.06	2.06	--
f(CO)	fraction pyro CO	.002	.075	.075	--
f(HC)	FRACTION PYRO (HC)	.172	.287	.287	--
F(smoke)	fraction pyro	0	--	--	--
$F(H_2O)$	fraction pyro H_2O	.71	1.07	1.07	--

n

FIRE DATA November 22, 1991

Fuel		polyvinylchloride (pvc) -CH-CH2- Cl	red oak C5H803.55	methane CH4	methanol CH3OH	propane C3H8	propanol C3H7OH
ρ	density kg.n3	1680	670		--	508	790
k	thermal conductivity w/m°K	.16	.213		.21	--	--
c_p	specific heat j/kg°K	1000	1368	2236	2500	1666	--
H_c*10^{-7}	combustion heat j/kg	1.64	1.78	5.3	2.0	4.7	3.1
H_v*10^{-6}	pyrolysis heat j/kg	2.47	1.8	1.8	1.1	1.1	.67
T_{ig}	Ignition temperature°K	510	730	813	480	723	730
T_f	Flame temperature°K	1200	1380	1400	1400	1475	1400
γ_s	air fuel ratio (stoi)	5.52	5.75	17.13	6.47	15.68	10.35
γ	air fuel ratio	9.6	8.9	36	13.5	30	21
ϵ	emissivity	1	.75	--	.42	--	.4
κ	absorption coef. m^{-1}	--	.53	1	1	2	1
χ	fraction heat release	.35	.75	.99	.993	.9	.98
χ_R	Fraction heat radiated	.15	.2	.15	.15	.3	.2
Δ	burn rate	--	.016	--	--	--	--
$f(CO_2)$	fraction pyro CO_2	.33	1.3	2.72	1.365	2.97	2.18
f(CO)	fraction pyro CO	.038	.01	.004	.001	.01	.005
f(HC)	FRACTION PYRO (HC)	.016	.005	0	0	--	--
F(smoke)	fraction pyro	.22	.018	.006	.006	.004	--
$F(H_20)$	fraction pyro H_20	.40	.58	2.25	1.125	1.636	1.2

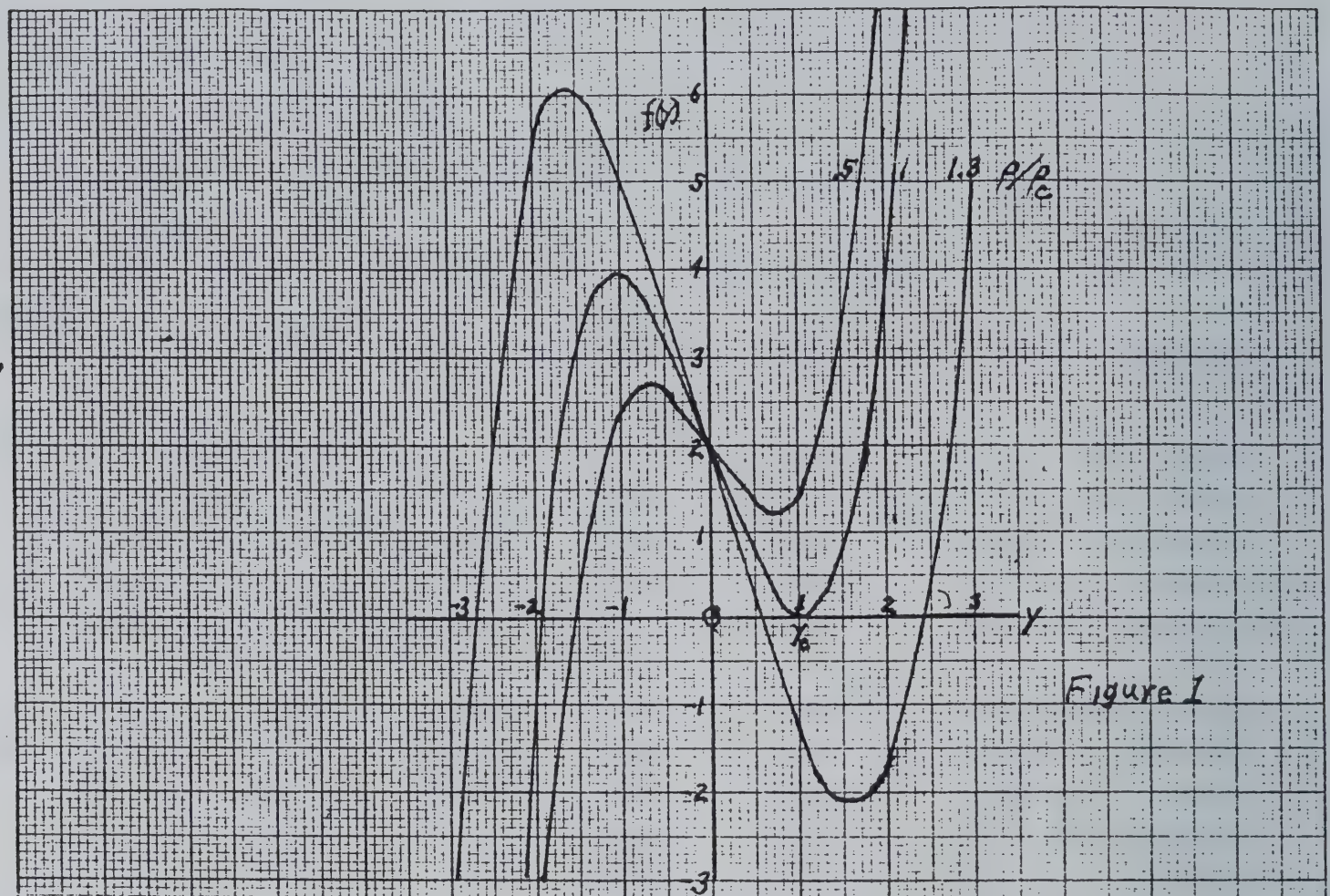

Figure 1

Figure 2

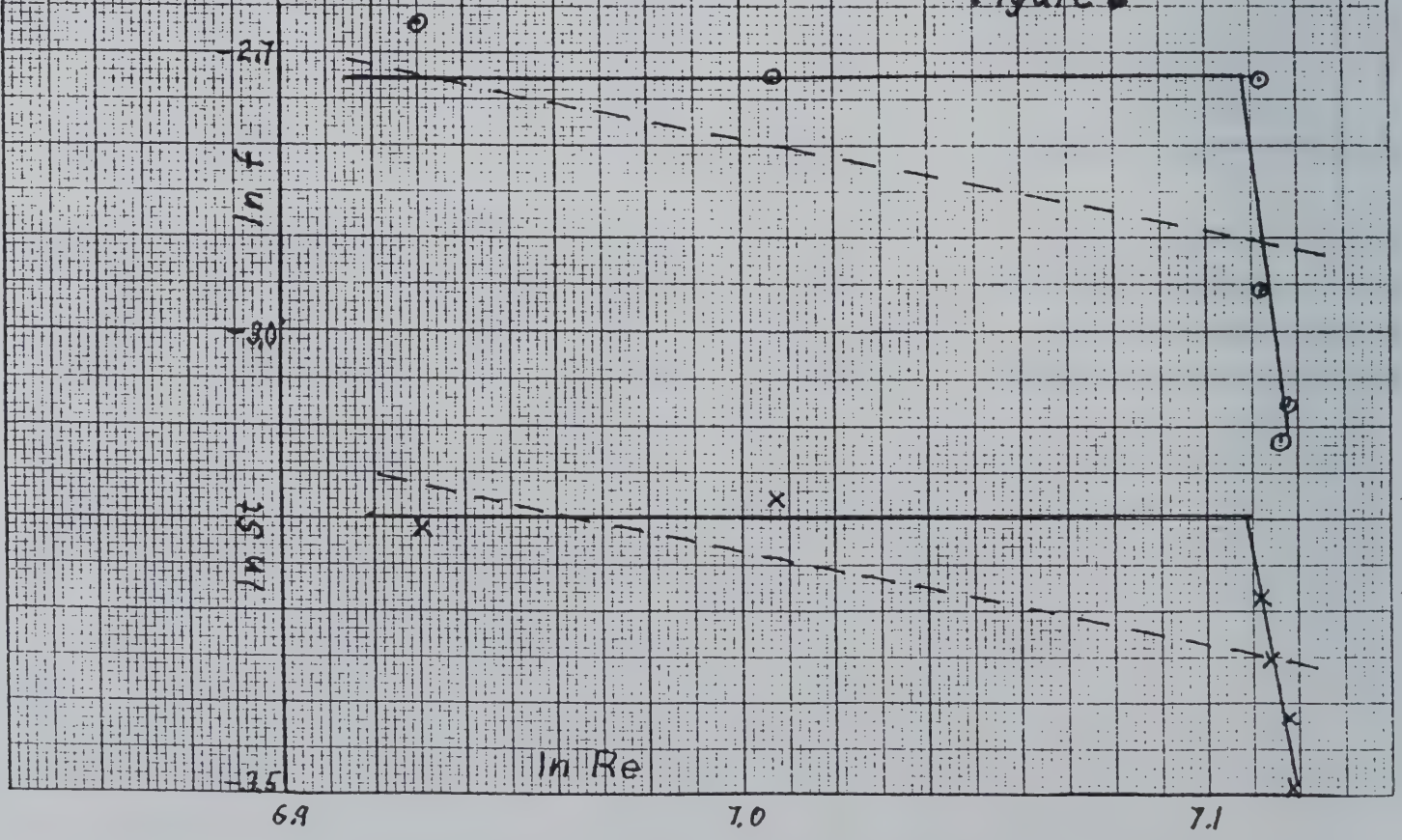

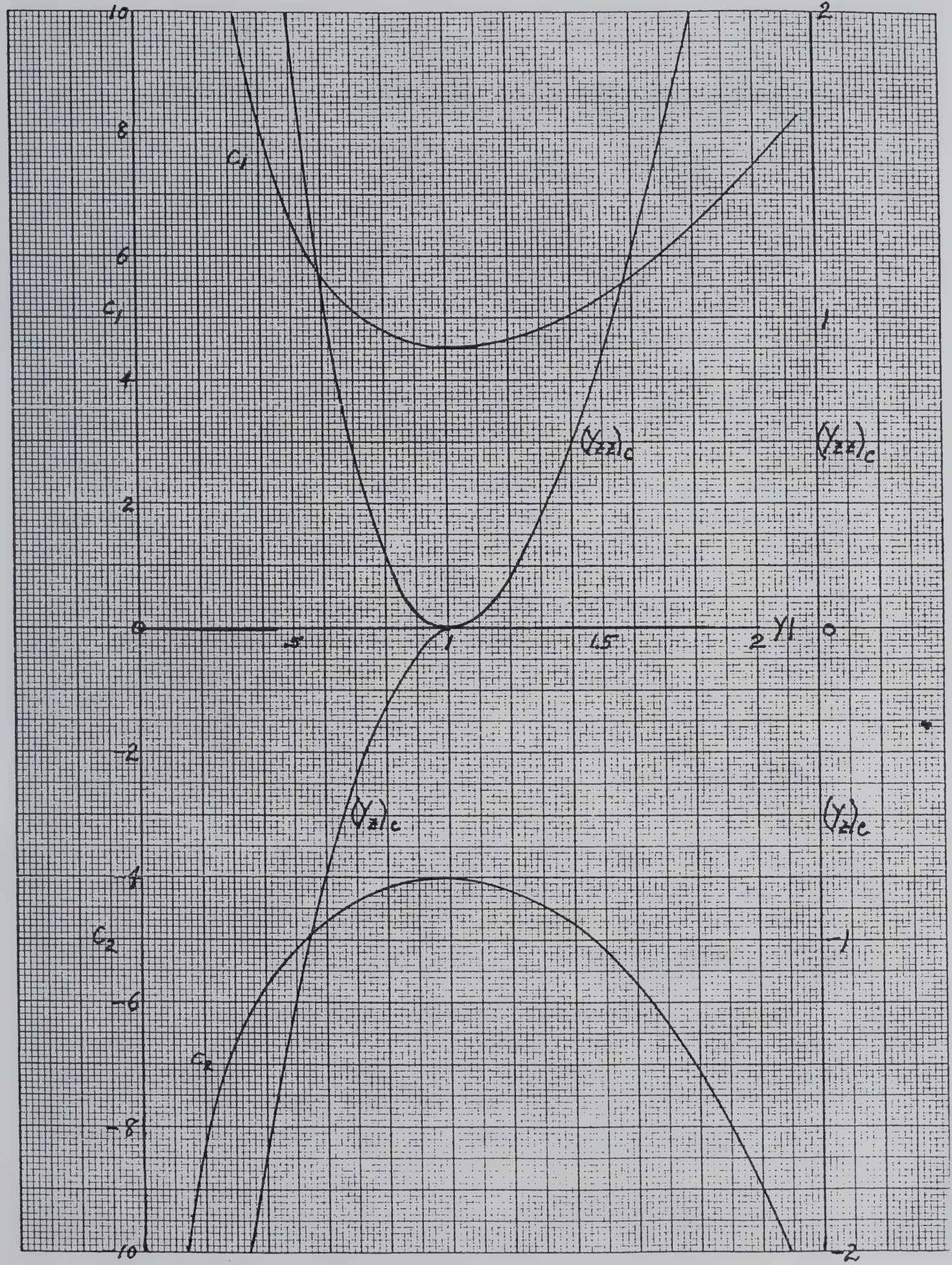

Figure 3

Task 2. Models for Turbulent Flame Chemistry and Radiation
(J. de Ris, L. Orloff)

Radiation from turbulent diffusion flames controls the burning rates of moderate and large-scale fires (1) and is, therefore, of central importance to the flammability problem. Recently, we have developed a global flame radiation model (2) which predicts the radiant fraction from buoyant turbulent (fuel-jet) diffusion flames in terms of the fuel's laminar flame smoke-point value. The model considers the separate roles of soot and gaseous radiation. The effective flame radiation temperature is predicted by the model in terms of the: 1) incompleteness of combustion, 2) radiant heat loss and 3) turbulent mixing, resulting in good agreement with experiment (3).

It is argued that the soot absorption coefficient (or soot volume fraction) is: 1) proportional to the turbulent macro-scale flow time in the soot formation region of the flames, and 2) inversely proportional to the chemical time for soot formation. The chemical time for soot formation is shown to be approximately proportional to the smoke-point heat release rate on the basis of the laminar flame smoke-point models of Kent (4) and Gulder (5). Markstein's general correlations (6,7) of smoke-points in terms of the stoichiometric oxidant to fuel mass ratio, S, and adiabatic stoichiometric flame temperature, T_{ad} for nitrogen diluted fuel and oxidant mixtures show that: 1) the soot formation is quite sensitive to S which controls the local velocity of the gas flowing through the diffusion flame toward the fuel side, while 2) the soot formation is relatively insensitive to T_{ad}. The latter result allows us to generalize the turbulent flame radiation model to include nitrogen diluted fuel mixtures and nitrogen diluted/oxygen enriched oxidants.

The predicted radiant fractions are in excellent agreement with experiment for different oxidant and fuel mixtures covering a wide range of flame sootiness. The model is tested against both axisymmetric (8) and planar (9) free-jet buoyant turbulent diffusion flames over a range of heat release rates. We are currently

applying the model to wall fire flames which have smaller radiant fractions due to: 1) convective heat loss to the surface, 2) significant dilution of the supplied fuel gases by products of combustion diffusing back toward the fuel source, and possibly 3) reduced macro-scale mixing times due to wall shear stress.

The model requires knowledge of the fuel smoke point which effectively characterizes the fuel's chemical structure. Methods are now available for evaluating the required smoke point of gaseous, liquid, and solid (charring and non-charring) fuels of interest.

By developing algebraic curve-fit formulas for the soot and gaseous emissivities, the model is self-contained and can be readily implemented using spread-sheet software.

References

1. de Ris, J.: Seventeenth Symp. (Int.) on Combustion, The Combustion Institute, Pittsburgh, PA (1979), 1003.

2. de Ris, J. and Orloff, L.: submitted to Combustion and Flame.

3. Markstein, G.H.: Comb. and Flame, 27, (1976), 51.

4. Kent, J.H.: Comb. and Flame, 63, 349-358 (1986).

5. Gulder, O.L.: Comb. and Flame, 78, 179-194 (1989).

6. Markstein, G.H.: Twenty-First Symp. (Int.) on Combustion, The Combustion Institute, Pittsburgh, PA (1987), 1107-1114.

7. Markstein, G.H.: Twenty-Second Symp. (Int.) on Combustion, The Combustion Institute, Pittsburgh, PA (1989), 363-370.

8. Orloff, L., de Ris, J., and Delichatsios, M.A.: Comb. Sci. and Tech., (1992) in press.

9. Markstein, G.H. and de Ris, J.: Twenty-Third Symp. (Int.) on Combustion, The Combustion Institute, Pittsburgh, PA (1991), 1685.

Task 3. Turbulent Flame Heat Transfer to Surfaces (G.H. Markstein)

The scientific understanding of wall-fire combustion and in particular the development of pertinent theoretical models (1-4) require experimental data on flame radiation so that these models can be applied to fires of hazardous scale where radiative energy transfer plays a controlling role. The purpose of the present work is to extend the range of such data beyond the upper limits of fuel sooting tendency and flame height attained in previous investigations (2,5-8). In the approach used here, wall fires of solid fuels are simulated by burning gaseous hydrocarbon fuels under steady-state conditions. The four fuels, methane, ethane, ethylene and propylene, are used to cover a sufficiently wide range of sooting tendency.

Initially, the study concentrated on the simulated overfire region by releasing the entire fuel flow from a horizontal slot burner placed adjacent to a vertical water-cooled metal plate (9,10) while more recent work (11) is concerned primarily with the pyrolysis region, simulated by supplying gaseous fuels from a water-cooled vertical sintered-porous-metal surface. The burner developed for this study consists of ten 132-mm-high and 380-mm-wide vertical porous-metal panels topped by a 660 mm high water-cooled solid-metal heat transfer plate divided into five similar segments. To approach two-dimensional flow conditions as closely as possible, water-cooled side walls of 150 mm depth are attached to the burner over the entire height of 1980 mm.

The water-cooling passages embedded in the porous metal and the heat transfer plate are instrumented with differential thermocouples for measurement of the total heat transferred to each panel and segment by the flame. Other instrumentation includes a wide-view-angle radiometer measuring total radiant emission and a slit scanning radiometer to determine the vertical distribution of radiant emission by horizontal slices across the wall fire.

In the slot-burner work (9,10) it was found that the radiative fraction of total heat release rate was reduced significantly by placing the burner adjacent to a water-cooled wall, compared to

values obtained with free-burning slot-burner or jet flames. This work also yielded dimensionless correlations of radiant emission as a function of height independent of heat release rate, by introducing a radiation flame-length parameter. The latter varied with the 1/2 power of heat-release rate, suggesting that flame heights are controlled primarily by radiant cooling rather than turbulent mixing, and implying a mean volumetric heat-release rate independent of fire size and fuel type.

Work with the porous-metal burner (11) showed that for any fixed fuel mass flux, the radiance N_o increases linearly with height, z, after an initial jump at the flame base. At fixed z, linear relationships between reciprocal radiance N_o^{-1} and reciprocal mass flux m''^{-1} were obtained. For methane and ethane these relationships held over the entire range of mass flux, while, for ethylene and propylene, an abrupt transition separating two regimes occurred at critical mass fluxes. The ordinate intercept N_∞, representing an asymptotic radiance, and the slope s of the linear relationship, are functions of height z. N_∞ and s^{-1} increase with fuel sooting tendency at fixed z.

Heat fluxes to the porous-metal panels decreased with increasing mass flux near the flame base, but were nearly independent of mass flux near the top portion of the porous-metal burner. These heat fluxes increased with fuel sooting tendency except for a reversed trend between methane and ethane. At sufficiently high mass flux, a jump of heat flux occurred at the junction between the porous-metal burner and the solid-metal heat transfer plate, and the heat flux increased further with height in this over-fire region. In this zone, the data were separated into a lower overlapping set for alkane fuels, methane and ethane, and a higher overlapping set for the alkenes, ethylene and propylene.

For a more complete understanding of wall-fire heat transfer, additional data are needed. In particular, separation of total heat flux to the wall into its radiative and convective components is an essential requirement for the development of a predictive theoretical model. Instrumentation for performing pertinent

measurements is currently being developed. However, preliminary estimates of the separation can be obtained from the current data. Figure 1 shows a plot of $\dot{q}''_r$ vs radiance N_o at a fixed mass flux $\dot{m}''$ and a fixed height z for the four fuels. Similar linear plots were obtained for other values of $\dot{m}''$ and z. The ordinate intercept, which represents the heat flux extrapolated to zero flame radiance, may be interpreted as the convective component of heat flux, while the slope multiplied by the radiance may be regarded as the radiative component for each fuel.

Intercepts as a function of mass flux for two heights are shown in Fig. 2 and Figure 3, which show that they decrease with increasing mass flux. This decrease is more pronounced at a height of 198 mm than at the greater height of 726 mm. A theoretical argument[12] shows that the slope should vary from a value of 1.8 π for optically thin to a value of π for optically thick isothermal flames. Figure 4 shows that at a height of 726 mm, the slope varies from 1.6 π (near optically thin) for low mass flux of 5 g/m^2s to about 1.0 π (optically thick) for high mass flux of 20 g/m^2s, while Fig. 5 shows that at a mass flux of 15 g/m^2s, the slope maintains the optically-thick value of 1.0 π over the entire height range. The new instrumentation will permit verification of this tentative interpretation, and may, in addition, indicate possible deviations from isothermal conditions, as well as blocking effects by a cold soot layer adjacent to the wall.

References

1. Kennedy, L.A. and Plumb, O.A.: Sixteenth Symposium (Int.) on Combustion, p. 1699, The Combustion Institute, 1977.

2. Ahmed, T. and Faeth, G.H.: Seventeenth Symposium (Int.) on Combustion, p. 1149, The Combustion Institute, 1979.

3. Tamanini, F.: Seventeenth Symposium (Int.) on Combustion, p. 1075, The Combustion Institute, 1979.

4. Delichatsios, M.A.: Nineteenth Symposium (Int.) on Combustion, p. 1075, The Combustion Institute, 1983, Combustion Science and Technology, 39, 195, 1984.

5. Orloff, L., de Ris, J., and Markstein, G.H.: Fifteenth Symposium (Int.) on Combustion, p. 183, The Combustion Institute, 1975.

6. de Ris, J. and Orloff, L.: Fifteenth Symposium (Int.) on Combustion, p. 175, The Combustion Institute, 1975.

7. Orloff, L., Modak, A.T., and Alpert, R.L.: Sixteenth Symposium (Int.) on Combustion, p. 1345, The Combustion Institute, 1977.

8. Quintiere, J., Harkleroad, M., and Hasemi, Y.: Combustion Science and Technology, 48, 191 (1986).

9. Markstein, G.H. and de Ris, J.: Twenty-Third Symposium (Int.) on Combustion, p. 1685, The Combustion Institute, 1991.

10. Markstein, G.H. and de Ris, J.: "Wall-Fire Radiant Emission. Part 1. Slot-Burner Flames, Comparison with Jet Flames," FMRC Technical Report, RC90-BT-2, August 1990.

11. Markstein, G.H. and de Ris, J., "Wall-Fire Radiant Emission. Part 2. Radiation and Heat Transfer from Porous-Metal Wall Burner Flames," 24th (Int.) Symposium on Combustion. (in press)

12. de Ris, J., Unpublished Memorandum, December 1990.

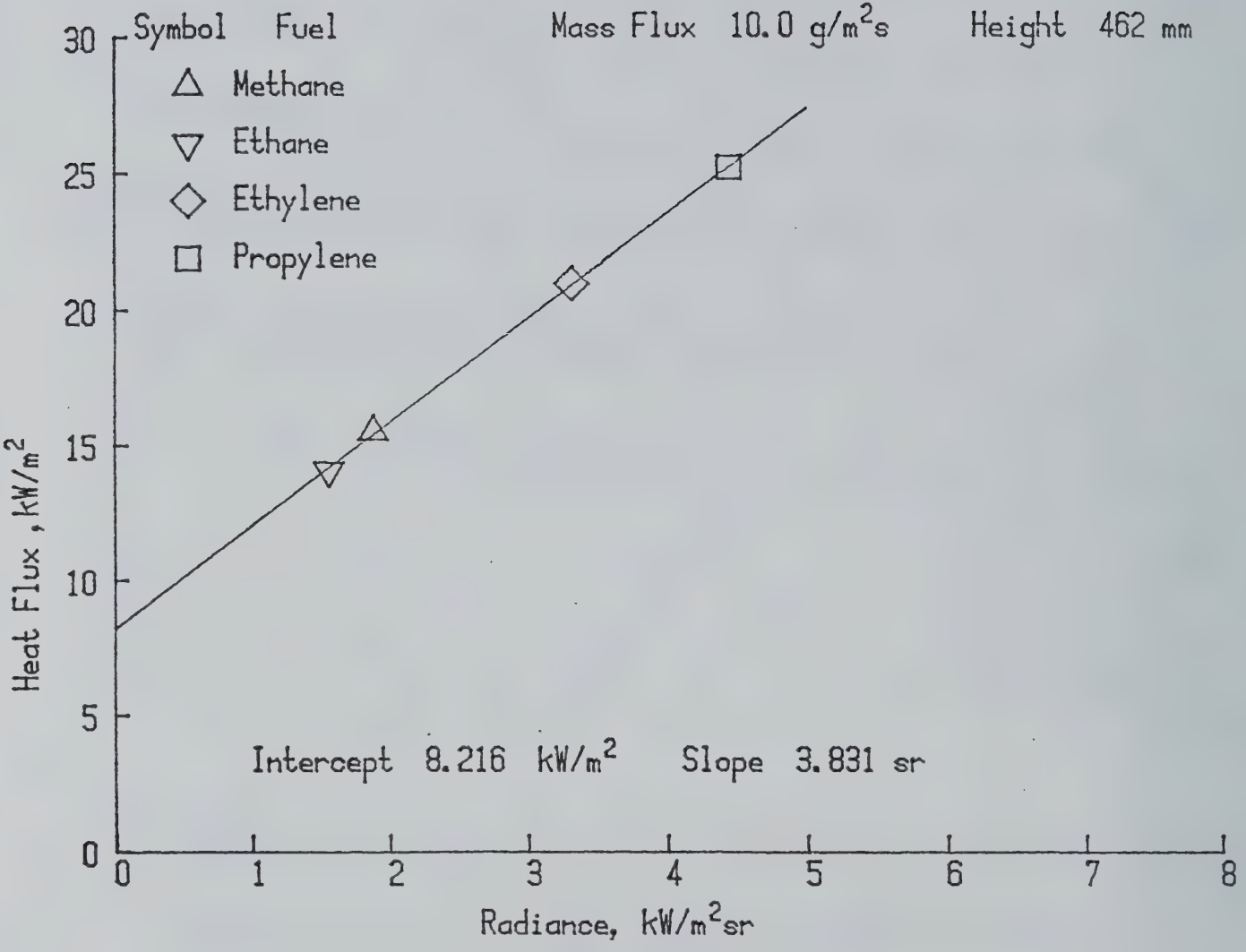

Fig. 1: Wall-fire heat flux vs. radiance for fixed mass flux and fixed height

Fig. 2: Intercept (representing convective heat transfer) vs. mass flux at a height of 198 mm.

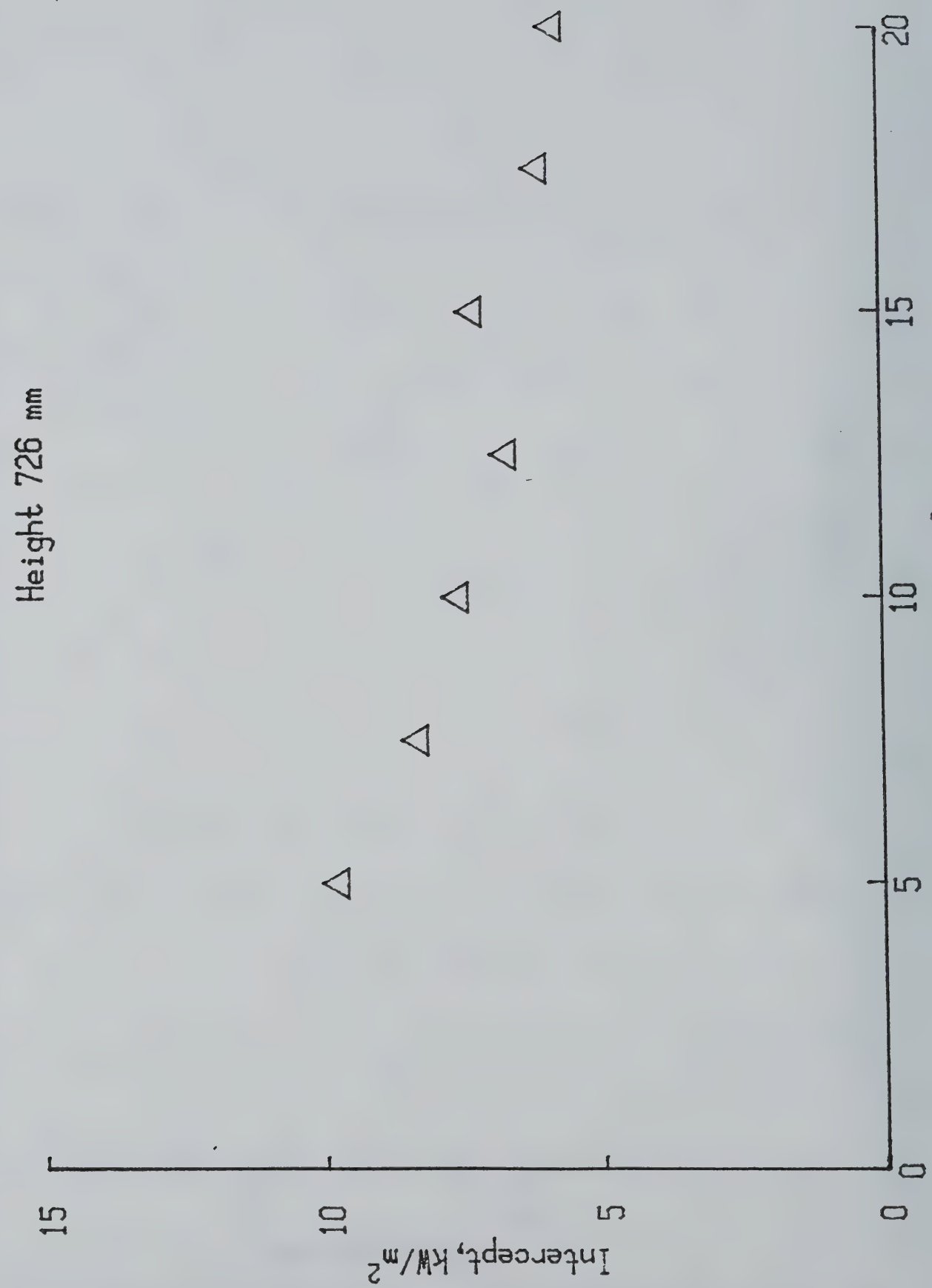

Fig. 3: Intercept vs. mass flux at a height of 726 mm.

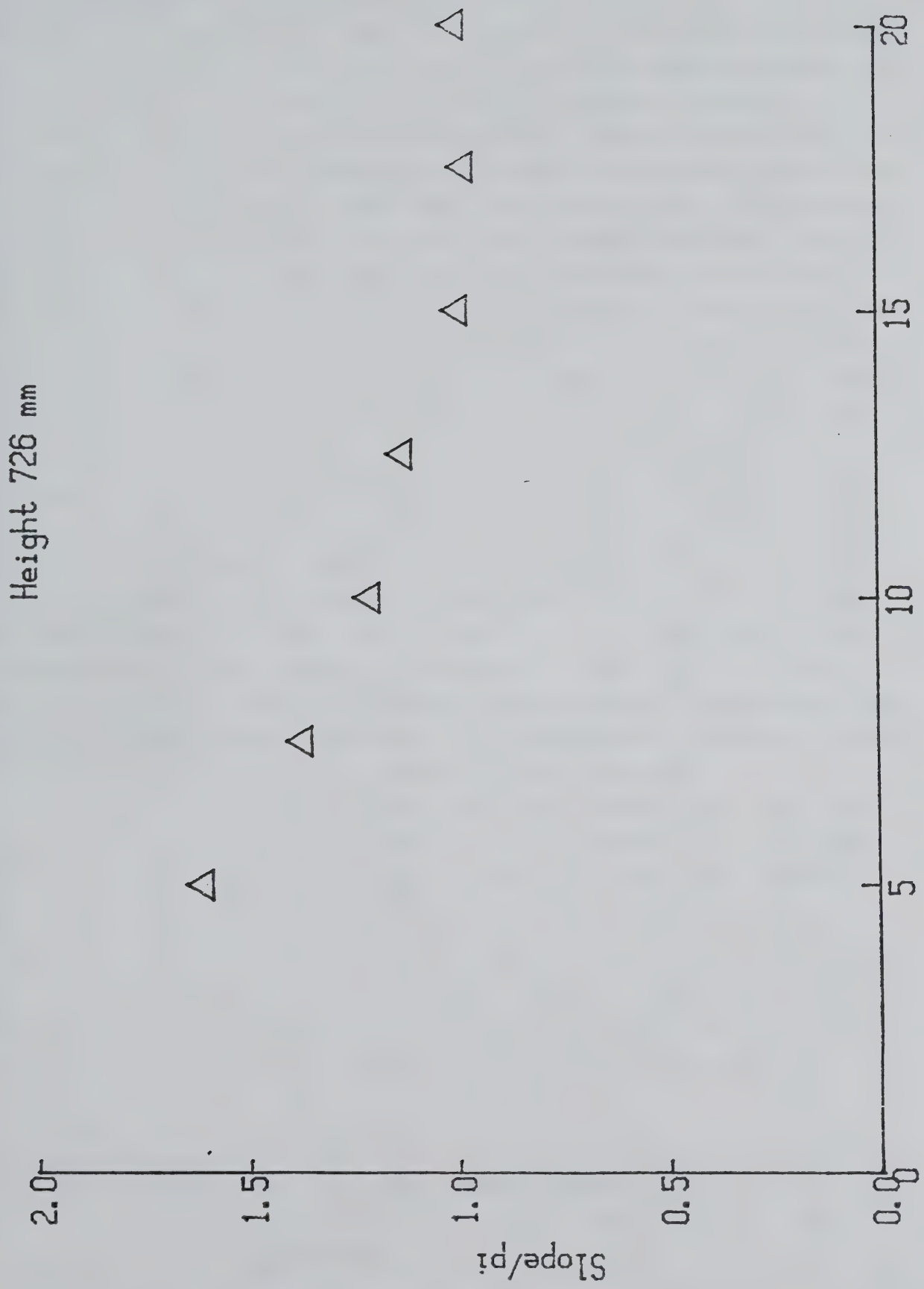

Fig. 4: Slope/π vs. mass flux at a height of 726 mm.

Fig. 5: Slope/π vs. height for a mass flux of 15 g/m^2s

Task 4. Measurement of Charring Fuel Smoke Points (J. de Ris, Xiaofang Cheng)

The objective of this task is to measure the smoke points of several charring solid materials by moving horizontal samples under a controlled CO_2 laser heat source, and to compare results with smoke points obtained by the existing vial technique, and correlate both results against measurements of incompleteness of combustion.

It is now well established that the smoke point of a material provides a direct measure of a material's flame sootiness and it is anticipated that the smoke point may also provide various other non-thermal damage[1] characteristics of a material. The smoke point also correlates the radiant fraction of the total heat release rate and the incompleteness of combustion of turbulent diffusion flames typical of fires. Clearly, the smoke point is a very important material flammability property which needs to be measured for practical fuels. It can readily be measured for gaseous, liquid and non-charring solid fuels which can be made to support a controlled steady laminar "candle-like" diffusion flame. The smoke point is defined as the maximum flame height which just does not emit smoke from the flame tip. A typical 10 cm high smoke-point flame requires a fuel supply rate of only 4×10^{-3} g/s. The small amount of material required for such measurements should make the smoke-point measurement particularly attractive to chemical industry researchers involved in developing new materials.

The major problem with using the smoke point as a material flammability property is the difficulty in measuring it for charring fuels. The pyrolysis rates of charring fuels are usually transient. The char produced during transient pyrolysis may chemically react with the pyrolysis gases causing them to change chemically and alter their smoke-point value. There is also the possibility that the pyrolysis vapors may change chemically when coming into contact with a heated surface before entering the

[1]Damage due to CO, soot particles and corrosive chemical compounds.

laminar candle-like flame. These issues need to be resolved as part of the development of a practical smoke-point test method.

Previously, as part of this grant, M.A. Delichatsios established that it is possible to measure the smoke-point of a charring fuel. He placed samples of PMMA, wood and neoprene in a small quartz vial and exposed the vial to a controlled quartz-halogen radiant heat source in our flammability research laboratory. By manually increasing and decreasing the radiant exposure, he obtained a preliminary smoke-point measurement for all three fuels. The PMMA value agreed with previous results obtained by Tewarson.

We have recently assembled an apparatus for measuring the smoke point of a charring material by slowly moving a horizontal slab under a focused beam from a CO_2 laser. By adjusting either the horizontal feed rate or CO_2 laser power we can control the height of the steady laminar flame. The flame height is measured by video camera while the smoke release is measured by its extinction of an electrically chopped IRLED optical beam passing across an exhaust chimney above the flame. A threshold circuit powers a light bulb seen by the video camera when the smoke release exceeds some specified small value.

Initial measurements of the smoke point for PMMA and two types of particle board show that the smoke-point flame height is independent of the horizontal feed rate. Greater feed rates require more laser power. A laser power of less than 70 W should be sufficient for all materials of interest.

The laser technique has the particular advantage of allowing the fuel gases to immediately enter the attached laminar flame without coming into contact with any neighboring hot surface, such as the mouth of a heated vial or other fuel holder. The flame remains well anchored to the fuel surface because of the intense flame to solid heat transfer characteristic of creeping flames.

We have now tested a new apparatus that can fully exploit this laser technique. The apparatus, shown in Figure 1, consists of a stationary glass-enclosure with perforated metal sheets on two sides and the top for air access. Experiments with fuel-gas

instead of a solid sample have proven the feasibility of stabilizing the laminar flame with parallel, perforated horizontal plates near the flame base, as suggested by a new theory for pulsating pool fires. Soot production when the flame height is above the smoke point is detected by a near-infrared LED beam while flame height is measured with a video camera.

Some results for PMMA and particleboard are shown in Figures 2, 3 and 4. A report is in preparation.

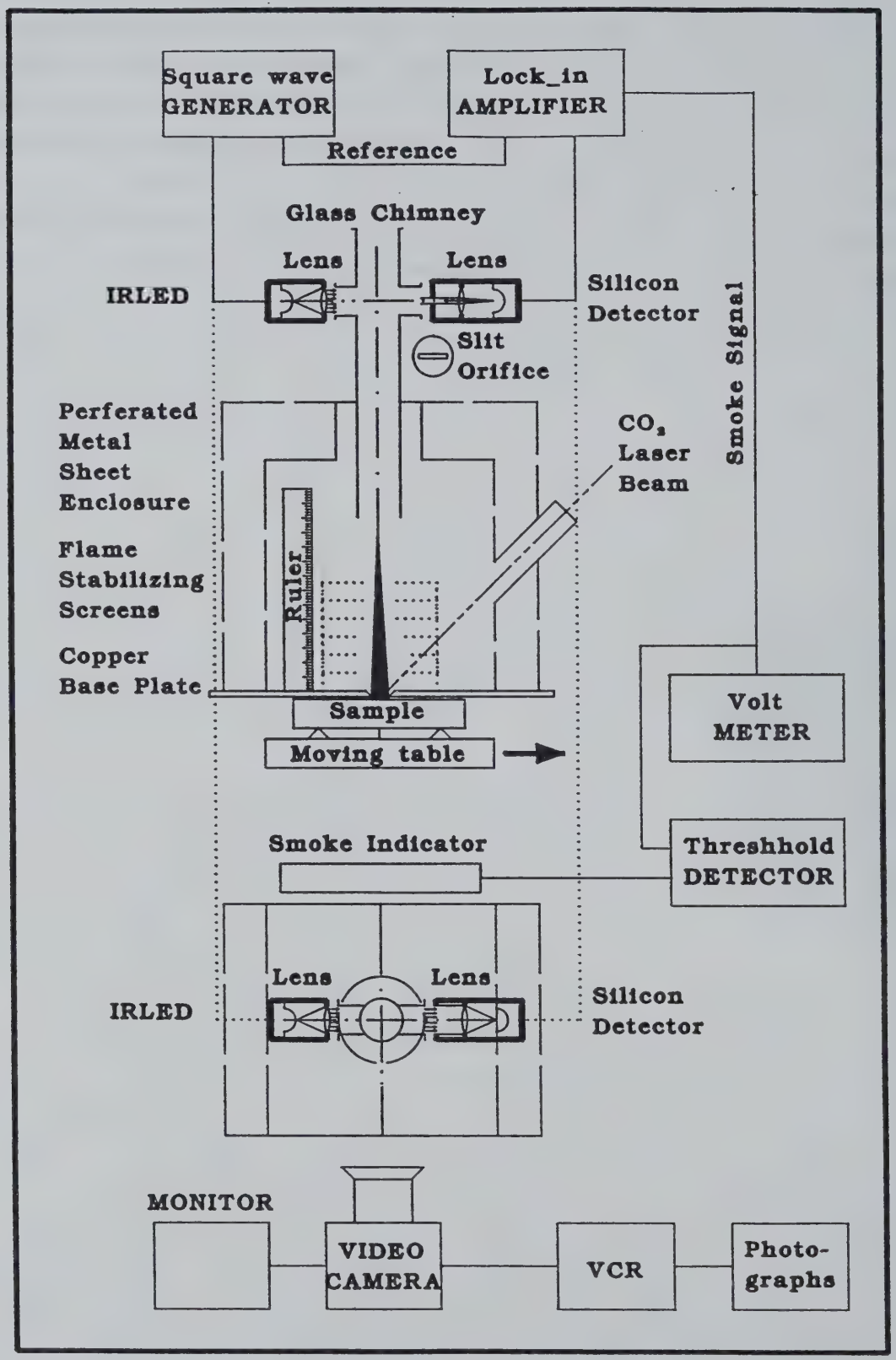
Square wave GENERATOR
Lock_in AMPLIFIER
Reference
Glass Chimney
Lens
Lens
IRLED
Silicon Detector
Slit Orifice
Smoke Signal
Perforated Metal Sheet Enclosure
CO_2 Laser Beam
Flame Stabilizing Screens
Ruler
Copper Base Plate
Sample
Moving table
Volt METER
Smoke Indicator
Threshhold DETECTOR
Lens
Lens
IRLED
Silicon Detector
MONITOR
VIDEO CAMERA
VCR
Photo-graphs

Figure 1

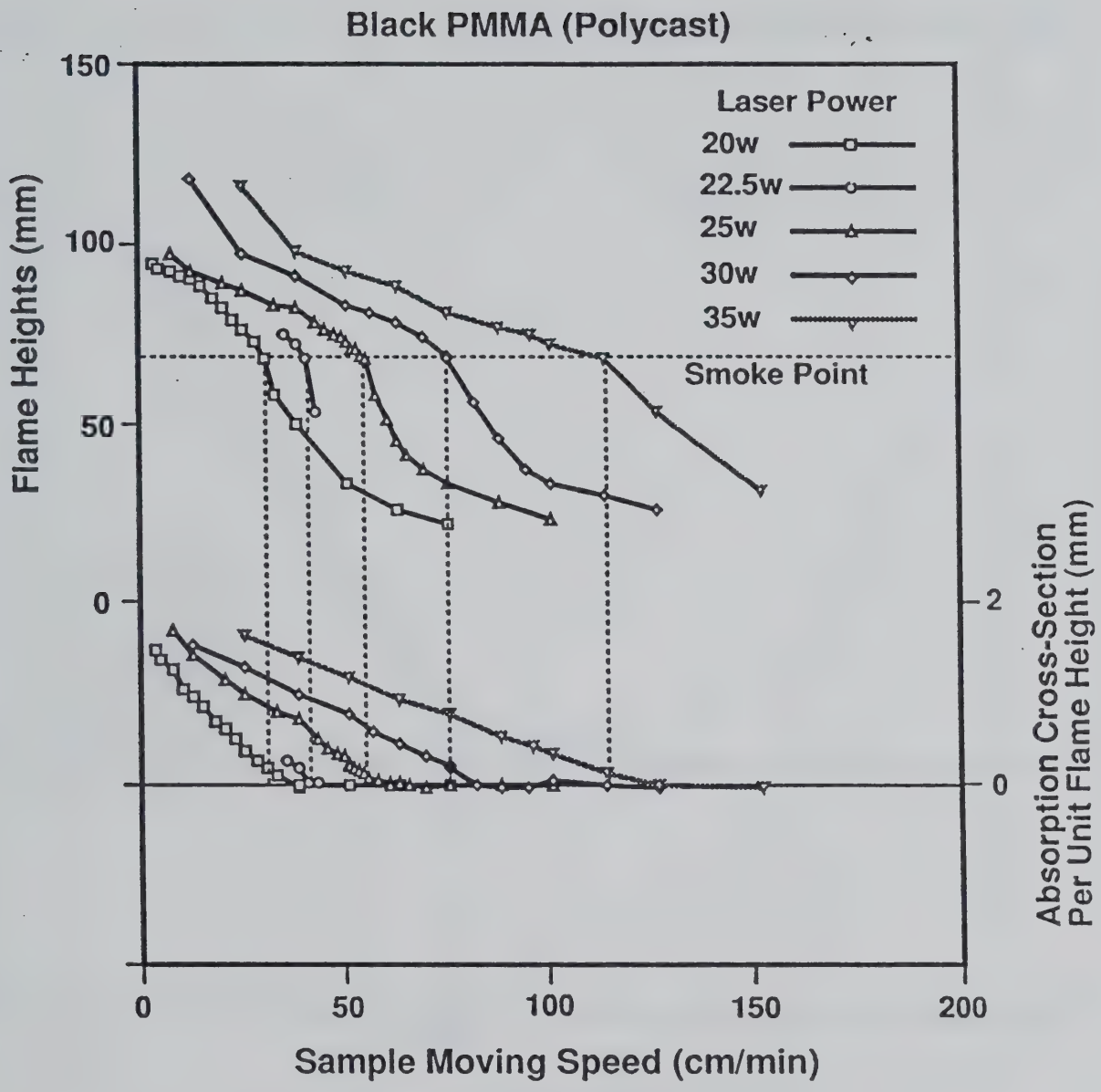
Black PMMA (Polycast)
Laser Power
20w
22.5w
25w
30w
35w
Smoke Point
Flame Heights (mm)
150
100
50
0
2
0
Absorption Cross-Section
Per Unit Flame Height (mm)
0
50
100
150
200
Sample Moving Speed (cm/min)

Figure 2

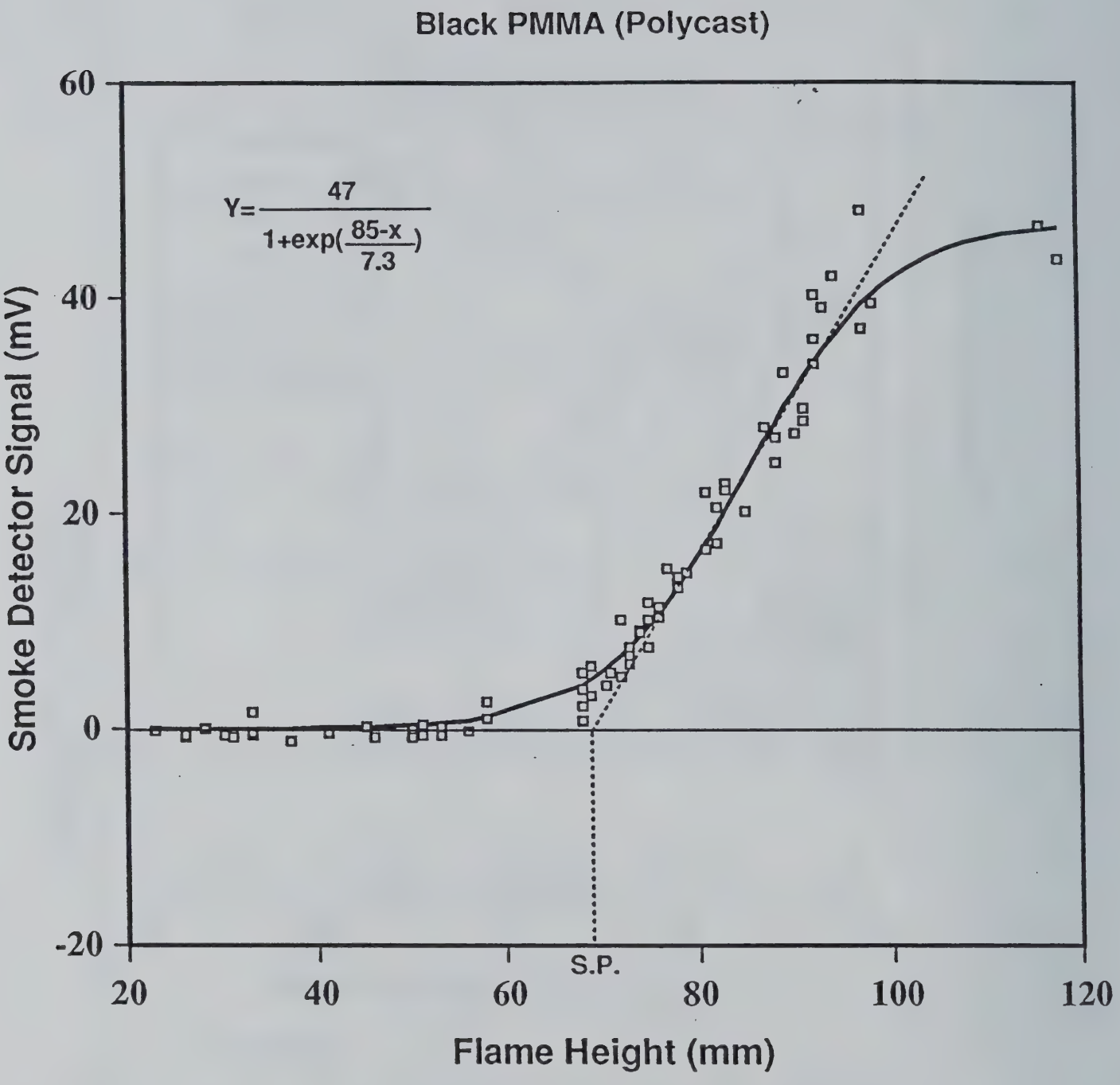
Black PMMA (Polycast)
Y= 47 / 1+exp((85-x)/7.3)
Smoke Detector Signal (mV)
60
40
20
0
-20
S.P.
20
40
60
80
100
120
Flame Height (mm)

Figure 3

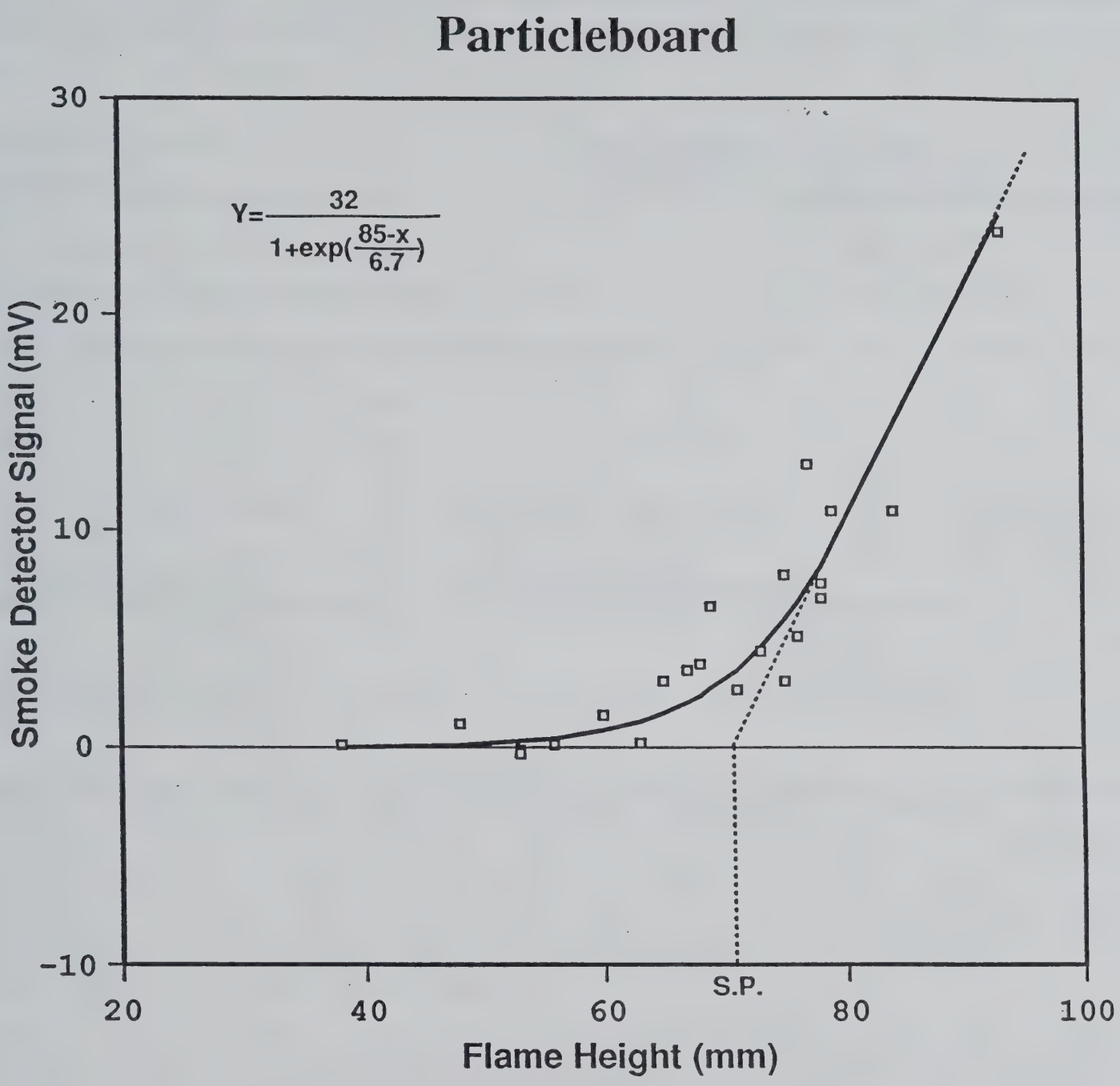
Particleboard
$Y=\frac{32}{1+\exp(\frac{85-x}{6.7})}$
Smoke Detector Signal (mV)
30
20
10
0
-10
20
40
60
80
100
S.P.
Flame Height (mm)

Figure 4

NIST-114
(REV. 6-93)
ADMAN 4.09

U.S. DEPARTMENT OF COMMERCE
NATIONAL INSTITUTE OF STANDARDS AND TECHNOLOGY

MANUSCRIPT REVIEW AND APPROVAL

(ERB USE ONLY)
ERB CONTROL NUMBER | DIVISION
PUBLICATION REPORT NUMBER: NIST-GCR-94-642 | CATEGORY CODE

INSTRUCTIONS: ATTACH ORIGINAL OF THIS FORM TO ONE (1) COPY OF MANUSCRIPT AND SEND TO THE SECRETARY, APPROPRIATE EDITORIAL REVIEW BOARD.

PUBLICATION DATE: June 1994 | NUMBER PRINTED PAGE

TITLE AND SUBTITLE (CITE IN FULL)

Prediction of Fire Dynamics

CONTRACT OR GRANT NUMBER: 60NANB1D1177

TYPE OF REPORT AND/OR PERIOD COVERED: Final and Fourth Quarterly Report June 28, 1992 - August 28, 1992

AUTHOR(S) (LAST NAME, FIRST INITIAL, SECOND INITIAL)

R.L. Alpert and J. de Ris
Factory Mutual Research Corporation
Norwood, MA 02062

PERFORMING ORGANIZATION (CHECK (X) ONE BOX)
[ ] NIST/GAITHERSBURG
[ ] NIST/BOULDER
[ ] JILA/BOULDER

LABORATORY AND DIVISION NAMES (FIRST NIST AUTHOR ONLY)

SPONSORING ORGANIZATION NAME AND COMPLETE ADDRESS (STREET, CITY, STATE, ZIP)

U.S. Department of Commerce
National Institute of Standards and Technology
Gaithersburg, MD 20899

PROPOSED FOR NIST PUBLICATION

[ ]	JOURNAL OF RESEARCH (NIST JRES)	[ ]	MONOGRAPH (NIST MN)	[ ]	LETTER CIRCULAR
[ ]	J. PHYS. & CHEM. REF. DATA (JPCRD)	[ ]	NATL. STD. REF. DATA SERIES (NIST NSRDS)	[ ]	BUILDING SCIENCE SERIES
[ ]	HANDBOOK (NIST HB)	[ ]	FEDERAL INF. PROCESS. STDS. (NIST FIPS)	[ ]	PRODUCT STANDARDS
[ ]	SPECIAL PUBLICATION (NIST SP)	[ ]	LIST OF PUBLICATIONS (NIST LP)	[X]	OTHER NIST-GCR-
[ ]	TECHNICAL NOTE (NIST TN)	[ ]	NIST INTERAGENCY/INTERNAL REPORT (NISTIR)		

PROPOSED FOR NON-NIST PUBLICATION (CITE FULLY) [ ] U.S. [ ] FOREIGN

PUBLISHING MEDIUM
[ ] PAPER [ ] CD-ROI
[ ] DISKETTE (SPECIFY)
[ ] OTHER (SPECIFY)

SUPPLEMENTARY NOTES

ABSTRACT (A 2000-CHARACTER OR LESS FACTUAL SUMMARY OF MOST SIGNIFICANT INFORMATION. IF DOCUMENT INCLUDES A SIGNIFICANT BIBLIOGRAPHY OR LITERATURE SURVEY, CITE IT HERE. SPELL OUT ACRONYMS ON FIRST REFERENCE.) (CONTINUE ON SEPARATE PAGE, IF NECESSARY.)

This report summarizes accomplishment of a Factory Mutual Research Corporation (FMRC) project on the Prediction of Fire Dynamics for the NIST grant period August 1991 through August 1992. Work performed under a subcontract by Professor H.W. Emmons on Ceiling-Jet Dynamics and on Development of Strategies for Performance Fire Codes is first described under Task 1. The accomplishment of three tasks performed at FMRC are then presented in summaries of Task 2-4. All of this work is aimed at the development of subroutines or algorithms that can be used in NIST/BFRL comprehensive computer models.

During the past year, there has been further progress in the development of predictive model for flame radiant heat flux and the development of a practical laboratory test method for measuring the smoke point of solid noncharring or charring materials. This progress should allow continuing improvements in the accuracy and applicability of fire propagation theories.

KEY WORDS (MAXIMUM OF 9; 28 CHARACTERS AND SPACES EACH; SEPARATE WITH SEMICOLONS; ALPHABETIC ORDER; CAPITALIZE ONLY PROPER NAMES)

algorithms; ceilings; computer models; fire codes; heat flux

AVAILABILITY

[X] UNLIMITED [ ] FOR OFFICIAL DISTRIBUTION - DO NOT RELEASE TO NTIS
[ ] ORDER FROM SUPERINTENDENT OF DOCUMENTS, U.S. GPO, WASHINGTON, DC 20402
[X] ORDER FROM NTIS, SPRINGFIELD, VA 22161

NOTE TO AUTHOR(S): IF YOU DO NOT WISH THIS MANUSCRIPT ANNOUNCED BEFORE PUBLICATION, PLEASE CHECK HERE. [ ]